Journal of Power Sources 246 (2014) 346–355

Contents lists available at ScienceDirect

Journal of Power Sources

journal homepage: www.elsevier.com/locate/jpowsour

Perovskite chromates cathode with resolved and anchored nickel nano-particles for direct high-temperature steam electrolysis

Shanshan Xu [a], Dehua Dong [c], Yan Wang [a,b], Winston Doherty [d], Kui Xie [a,b,*], Yucheng Wu [a,b]

[a] Department of Energy Materials, School of Materials Science and Engineering, Hefei University of Technology, No. 193 Tunxi Road, Hefei, Anhui 230009, China
[b] Key Laboratory of Advanced Functional Materials and Devices of Anhui Province, Hefei University of Technology, No. 193 Tunxi Road, Hefei, Anhui 230009, China
[c] Fuels and Energy Technology Institute, Curtin University of Technology, 1 Turner Avenue, Technology Park, WA 6102, GPO Box U1987, Perth, WA 6845, Australia
[d] School of Applied Sciences and Engineering, Gippsland Campus, Monash University, Churchill 3842, Victoria, Australia

HIGHLIGHTS

- Ni nanoparticles are anchored on cathode skeleton for direct steam electrolysis.
- The exsolution of Ni nanoparticles significantly enhance cathode performances.
- The synergy of Ni and ceramic cathode leads to stability of steam electrolysis.

ARTICLE INFO

Article history:
Received 20 June 2013
Received in revised form
22 July 2013
Accepted 24 July 2013
Available online 3 August 2013

Keywords:
Doped lanthanum chromates
Nickel
Steam electrolysis
Electrochemical performance
Solid oxide electrolyzer

ABSTRACT

Doped lanthanum chromates are now commonly used to prepare composite cathodes for direct steam electrolysis. However, the limitation of electrochemical performances and cell current efficiency by insufficient electro-catalytic activity is a major challenge. This paper reports the use of reversibly exsolved catalytic metallic Ni nano-particles on A-site deficient and B-site excess perovskite $(La_{0.75}Sr_{0.25})_{0.95}(Cr_{0.8}Ni_{0.2})_{0.95}Ni_{0.05}O_{3-\delta}$ (LSCNNi), in order to achieve an activity-enhanced composite cathode via high-temperature reduction under reducing atmospheres. The electrical properties of the ceramic are investigated methodically and correlated with the performances of the composite electrodes in symmetric and electrolysis cells. XRD, SEM, EDS and XPS results, confirm that the exsolution or dissolution of nano metallic catalyst is reversible in redox treatment cycles. The Faradic efficiency reaches approximately 80% for the LSCNNi cathode with the flow of 5%H_2/Ar. Ultimately, the unified effect of metallic catalyst and redox-stable ceramic produce striking redox stability as well as electrochemical performances of the titled composite cathode. The results signify that the composite cathode with exsolved nickel nano-particles, is a good potential fuel electrode for direct steam electrolysis in an oxygen-ion conducting solid oxide electrolyzer.

1. Introduction

There is a daily increasing need for clean and renewable energy resources owing to global climate change and environmental problems associated with combustion of fossil fuels [1–3]. Hydrogen is a leading alternative fuel candidate, because of its huge potential to address the threats of environmental and energy security issues inherent in combustion of fossil hydrocarbon fuels [4–7]. Steam can be electrolyzed into hydrogen and oxygen under the driving of external electricity, using an oxide-ion-conducting solid oxide electrolyzer (SOE). Reduction of H_2O molecule into H_2 occurs at the cathode electrochemically under an externally applied potential. The oxygen-ion conducting electrolyte transports the O^{2-} to the anode compartment, where O_2 gas is formed and released [2,8–10]. A SOE is the reverse running of a solid oxide fuel cell (SOFC); it is a promising electrochemical device that converts electrical energy directly into chemical energy as a result of which it has attracted a great deal

* Corresponding author. Department of Energy Materials, School of Materials Science and Engineering, Hefei University of Technology, No. 193 Tunxi Road, Hefei, Anhui 230009, China.
E-mail addresses: xiekui@hfut.edu.cn (K. Xie), ycwu@hfut.edu.cn (Y. Wu).

0378-7753/$ – see front matter © 2013 Elsevier B.V. All rights reserved.
http://dx.doi.org/10.1016/j.jpowsour.2013.07.082

of interests [11–14]. Steam electrolysis is energy-efficient and promising because the heat at high temperatures partly offers the energy for steam dissociation and hence leads to favorable kinetics and thermodynamics [2,15]. A conventional electrode material Ni/YSZ (yttria-stabilized zirconia) has been preferentially used as the composite cathode in an oxide-ion-conducting SOE for high-temperature steam or carbon dioxide electrolysis [16,17]. However, the constant passing of a significant concentration of reducing gas over Ni to avoid its oxidation, makes the Ni/YSZ cermet unstable during redox cycles. In addition, poor redox cycling performance and large thermal expansion coefficients are common disadvantages of the conventional Ni/YSZ cathode [18–20]. The perovskites based on $LaCrO_3(La_{1-x}Sr_x)(Cr_yM_{1-y})O_3$ (M = Mn, Fe, Ni and Co), for example, have been investigated and proved to be promising materials for high temperature SOFC anodes [21–26]. Recently, Irvine et al. demonstrated the feasibility of direct steam electrolysis based on an LSCM/SDC cathode without the flow of reducing gas over the electrode [5]. In recent times, we have also established that the direct electrolysis of CO_2 could be achieved to produce CO and O_2 in an oxygen-ion conducting solid oxide electrolyzer based on LSCM cathode without flowing reducing gas over it. However, the insufficient electro-catalytic activity of the LSCM ceramic cathode still restricts the Faradic current efficiency [24]. In our previous work, in order to address the limited catalytic activity of the LSCM cathode, iron nanoparticles were loaded, unto the composite cathode to improve electro-catalytic performance in the direct steam electrolysis [10]. As expected, the iron catalyst significantly enhanced the electrode performance and the current efficiency. However, it was difficult to control catalyst morphology on the substrate and long-term operation would cause catalyst agglomeration and, therefore, performance degradation. An alternative method is to incorporate the catalyst as a dopant within a host lattice during material synthesis in air, which is then exsolved on the surface in the form of catalytic and anchored metallic nano- or micron-particles under reducing atmospheres. Upon re-oxidation, the dopant may be re-incorporated into the host lattice, yielding a regenerative catalyst. Accordingly, the agglomeration of exsolved metallic nano-particles on the substrate surface could be avoided by periodically exposing the material to oxidizing atmospheres.

$La_{1-x}Sr_xCr_{1-y}Ni_yO_{3-\delta}$ perovskites have been reported as anodes for methane steam reforming process and proved tolerant of redox cycles [27,28]. In the present study, $(La_{0.75}Sr_{0.25})_{0.95}(Cr_{0.8}Ni_{0.2})_{0.95}Ni_{0.05}O_{3-\delta}$ perovskite with A-site deficiency and B-site excess was designed to tailor a composite nano-sized Nickel/$La_{0.75}Sr_{0.25}Cr_{0.8}Ni_{0.2}O_{3-\delta}$ (Ni/LSCN) through a reversible exsolution of nickel nano-particles, anchored on the surface of LSCN via a treatment under a high-temperature reducing atmosphere. The anchored Ni particles are expected to improve the electro-catalytic kinetics and the high-temperature stability of nickel nano-particles. The reversibly exsolved nickel metallic nano-particles are beneficial for the steam electrolysis, and it can re-incorporate into the substrate upon oxidation at high temperatures, which not only avoids the catalyst agglomeration but also enables the excellent cycling performances of the ceramic composite cathodes. In this work, we systematically studied the electrical properties of LSCN and LSCNNi and further correlate with the electrochemical properties of the cathodes. Steam electrolysis with cathodes based on LSCN and LSCNNi was investigated with and/or without reducing gas flowing over them, respectively. An 11-h test was performed to verify the stability of the LSCNNi composite cathode for direct steam electrolysis.

2. Experimental

All the chemicals used in this experiment were of analytical grade and purchased from SINOPHARM Chemical Reagent Co., Ltd (China). The LSCN and LSCNNi powders were synthesized by a traditional solid-state reaction method [27]. Stoichiometric amounts of La_2O_3, $SrCO_3$, Cr_2O_3, and NiO were mixed in acetone and ball-milled by zirconia balls for 5 min. The dried powders were pressed into pellets. The pellets were sintered at 1300 °C for 10 h and subsequently at 1500 °C for 5 h in air followed by grinding into powders. The $La_{0.8}Sr_{0.2}MnO_{3+\delta}$ anode powders were prepared in the same way and treated at 1100 °C for 3 h in air. The oxidized LSCN and LSCNNi powders were then reduced at 1200 °C for 6 h in 5%H_2/Ar. The re-oxidation of the samples was carried out at 1000 °C for 3 h in air. The phase of the prepared powders were analyzed using X-ray diffraction (Cu K_α, XRD, $2\Theta = 3°$ min^{-1}, D/MAX2500V, Rigaku Corporation, Japan) with 2Θ ranging from 10 to 90°. The microstructures of the oxidized and reduced samples were observed by a Scanning Electron Microscope (SEM, JSM-6490LV, JEOL Ltd, Japan) equipped with Energy Dispersive Spectroscopy (EDS). The valence states of elements in the oxidized and reduced samples were determined using an ESCALAB250 spectrometer with Al Kα (1486.6 eV) radiation source. Thermogravimetric analysis (TGA) of the oxidized and reduced samples was also performed in air from room temperature to 800 °C. An appropriate amount of LSCN and LSCNNi powders were pressed into a bar and sintered at 1500 °C for 5 h in air for a conductivity test. The conductivity of the samples were tested in air using the DC four-terminal method from 20 to 800 °C with the conductivity recorded at a step of 0.4 °C using an online system. The dependence of the conductivity on the oxygen partial pressure, which was adjusted by the flow rate of the dry 5% H_2/Ar, was tested at 800 °C within the range of $0.2–10^{-18}$ atm. The oxygen partial pressure (log PO_2) and the conductivity were recorded using an online oxygen sensor (1231, ZrO_2-based oxygen sensor, Noveltech, Australia) and an online multi-meter (Keithley 2000, Digital Multimeter, Keithley Instruments Inc., USA), respectively.

A group of 1-mm-thick 8YSZ disks were prepared by dry-pressing 8YSZ powders into green disks with a diameter of ~20 mm, followed by sintering in air at 1500 °C for 10 h. The two surfaces of the obtained YSZ electrolyte were mechanically polished and ultrasonically cleaned in ethanol and distilled water. The composite electrode LSCN/YSZ, LSCNNi/YSZ and LSM/YSZ slurries, were prepared by mixing the YSZ powders with the corresponding electrode powders at a weight ratio of 35:65 in alpha-terpineol with a cellulose additive. The electrolyzers were assembled by printing the electrode slurries onto the YSZ electrolyte in symmetric positions with an area of 1 cm^2, followed by a heat treatment at 1100 °C for 3 h in air. The current collection layer was constructed by painting silver paste (SS-8060, Xinluyi, Shanghai, China) on both electrode surfaces. The external potential was applied using a silver electrical wire (0.1 mm in diameter), which was connected with the current collectors using silver paste (DAD87, Shanghai Research Institute for Synthetic Resins) and heated at 550 °C for 30 min in air.

The symmetric cells based on the LSCN/YSZ and the LSCNNi/YSZ electrodes were prepared as described elsewhere [24]. The AC impedance of the two kinds of symmetric cells was tested at different hydrogen concentrations at 800 °C using an electrochemical station (IM6, Zahner, Germany). All flow rates of the gases were set as 50 ml min^{-1} using mass flow meters (D08-3F, Sevenstar, Beijing, China). For the steam electrolysis, the single solid oxide electrolyzer was sealed to a homemade testing jig using ceramic paste (JD-767, Jiudian, Dongguan, China) for electrochemical measurements. The steam electrolysis by the solid oxide electrolyzer based on the LSCN/YSZ and LSCNNi/YSZ composite cathodes was tested under different external potentials at 800 °C in 3%H_2O/5%H_2/Ar and 3%H_2O/Ar, respectively. The AC impedance spectroscopy and the current-versus-voltage curve (I–V curve) of the SOEs were recorded when the cathodes were exposed to the flowing stream

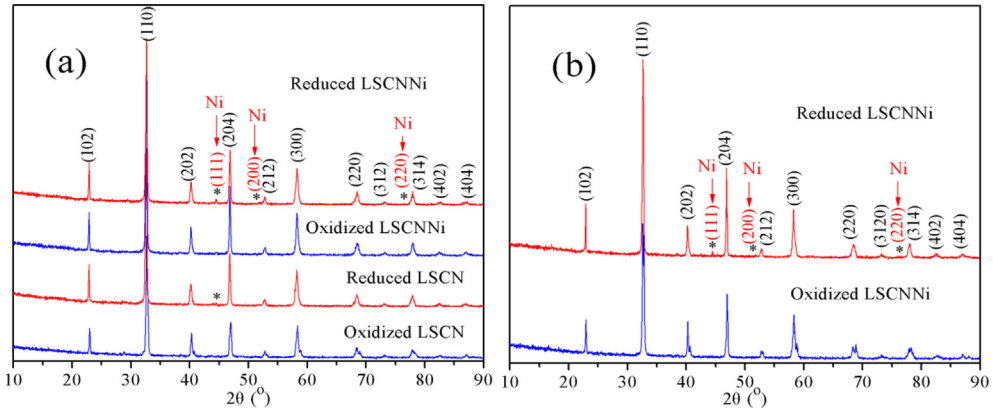

Fig. 1. XRD patterns of the prepared powders using the solid-state reaction method followed by a heat treatment at 1500 °C for 5 h in air and reduced at 1200 °C for 2 h in 5%H_2/Ar: (a) LSCN and LSCNNi samples; (b) Re-oxide LSCNNi and Re-reduced LSCNNi samples.

and the anodes to static air at 800 °C. The hydrogen concentration of the output gas from the cathode was analyzed using an online gas chromatograph (GC9790II, Fuli, Zhejiang, China).

3. Results and discussion

Fig. 1 presents the XRD patterns of the LSCN and LSCNNi for both the oxidized and reduced samples. As shown in Fig. 1(a), the XRD patterns of the oxidized samples confirm the single phase of the perovskite LSCN and LSCNNi powders, whereas the reduced samples are the mixture of two phases as the nickel metal's second phase is observed. Furthermore, the peak referring to nickel is considerably weak for the reduced LSCN sample, indicating that the effect of nickel exsolution from perovskite lattice is not sufficient in LSCN. Thereby, the exsolution of nano-particles may have negligible contribution to the improvement of the electro-catalytic performance. In contrast, the exsolution of nickel is obvious in the reduced LSCNNi sample, which suggests that the A-site deficiency and B-site excess of the perovskite are favorable for the nickel exsolution from lattice. In order to investigate the reversibility of exsolution, the reduced LSCNNi powders are further treated in air and then reduced again. As shown in Fig. 1(b), the corresponding XRD patterns confirm that the metallic nickel reversibly incorporates into the bulk to develop a single phase LSCNNi upon oxidation and the metallic nickel is repeatedly produced from the reduction of LSCNNi to form a Ni/LSCN matrix. This demonstrates the good reversible exsolution of the Ni metals from LSCNNi ceramic. The redox tests would indicate that the composite cathode based on LSCNNi ceramic is expected to demonstrate good cycling performances during oxidation and reduction. SEM and EDS results are employed to further characterize the oxidized and reduced samples. Fig. 2(a) and (b) respectively presents the microstructures of the oxidized LSCN pellet sintered at 1500 °C and the reduced LSCN pellet at 1200 °C. The grain size of the oxidized LSCN is approximately 2–3 μm and remains unchanged even under extremely reducing atmosphere. The surface of the reduced LSCN substrate does not show the presence of nickel nano-particle. The EDS image shows uniform distribution of all the elements in the reduced LSCN substrate. This, as previously discussed, indicates insufficient effect of nickel exsolution. Therefore, the Ni nano-particles are difficult to observe on the surface of LSCN. In comparison, Fig. 2(c) shows that the grain size of the oxidized LSCNNi is similar to that of LSCN. However, the nano-sized nickel particles exsolved from the reduced LSCNNi and anchored on the LSCN surface are observable as evident in Fig. 2(d), which the Ni mapping of the EDS patterns further confirmed. In addition, the La, Sr, Cr and O elements are evenly distributed. The nickel nano-particles fortified composite (LSCNNi) cathode is expected to show higher electro-catalytic properties compared to the bare LSCN cathode.

In order to further validate the elemental valence change of the samples, XPS analysis is performed to test the oxidized and reduced samples. The results reveal that there is no valence change before and after the reduction of La and Sr elements. The $Cr^{3+/4+}$ and Cr^{6+} featured in the oxidized LSCN and LSCNNi samples as can be seen in Fig. 3(a1) and (c1). There should be no +6 state of Cr in ABO_3 structure; however, the adsorbed atmospheric oxygen on the sample surface would probably oxidize the surface Cr^{4+} into Cr^{6+}, which is also confirmed by the signal of O_2^- caused by adsorbed oxygen as

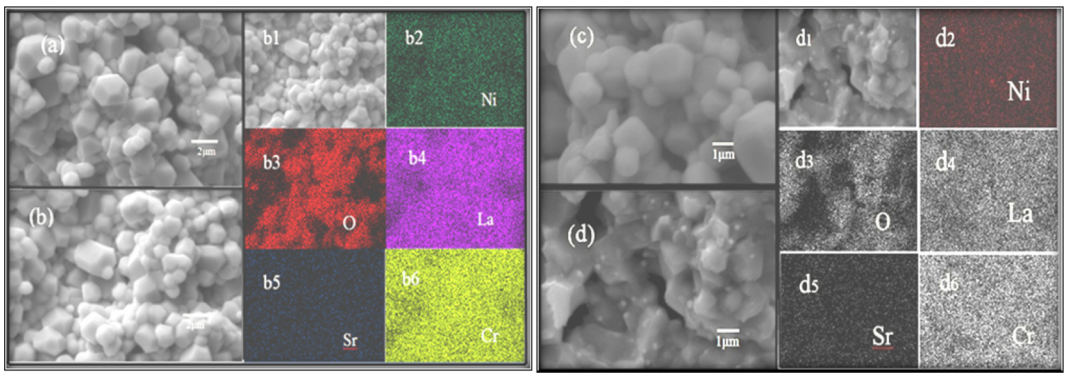

Fig. 2. SEM and EDX images of (a) oxidized LSCN; (b) reduced LSCN; (c) oxidized LSCNNi0.05 and (d) reduced LSCNNi samples.

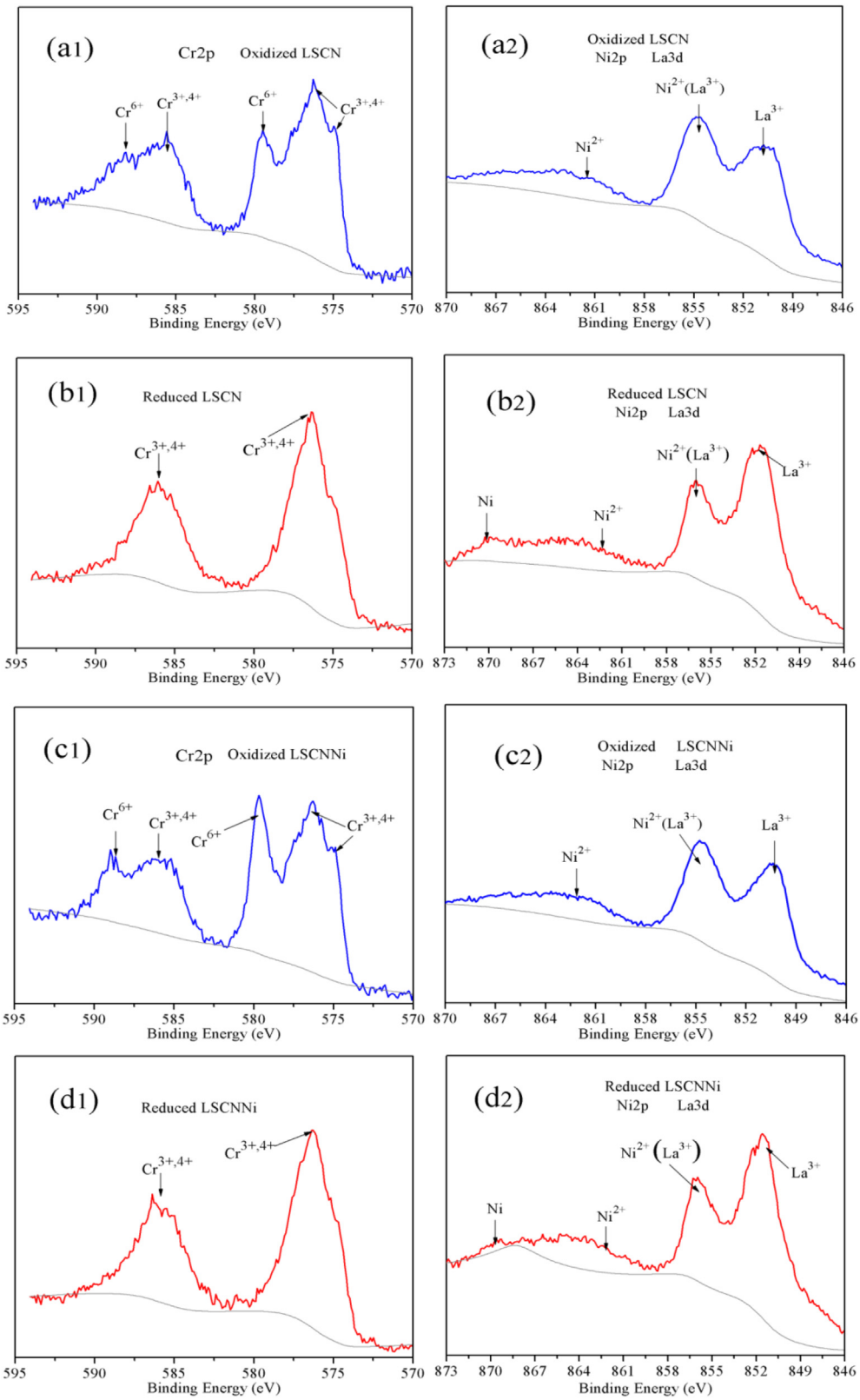

Fig. 3. XPS results of Cr (a1), Ni (a2) in oxidized LSCN; Cr (b1), Ni (b2) in reduced LSCN; Cr (c1), Ni (c2) in oxidized LSCNNi and Cr (d1), Ni (d2) in reduced LSCNNi samples.

shown in Fig. S1. The Cr^{6+} is reduced to Cr^{3+}, and only $Cr^{3+/4+}$ is observed in the reduced LSCN and LSCNNi samples as evident in Fig. 3(b1) and (d1). As evident in Fig. 3(a2) and (c2), the peaks of Ni^{2+} and La^{3+} overlap and only Ni^{2+} is observed for the oxidized samples. In contrast, both Ni^{2+} and Ni coexist in the reduced samples as shown in Fig. 3(b2) and (d2). The Ni element in oxidized samples is at +2 oxidation state while it exists in the form of Ni^{2+} and Ni in reduced samples. This further confirms the exsolution of metallic Ni

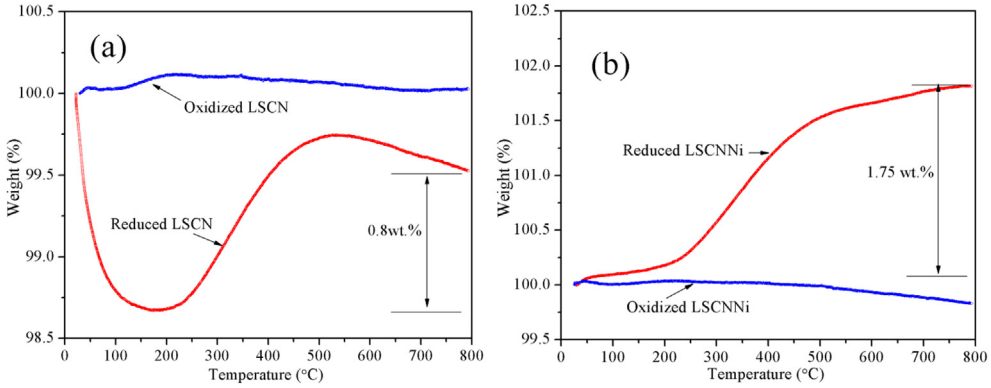

Fig. 4. TGA of the oxidized and reduced LSCN (a) and LSCNNi (b) from room temperature to 800 °C.

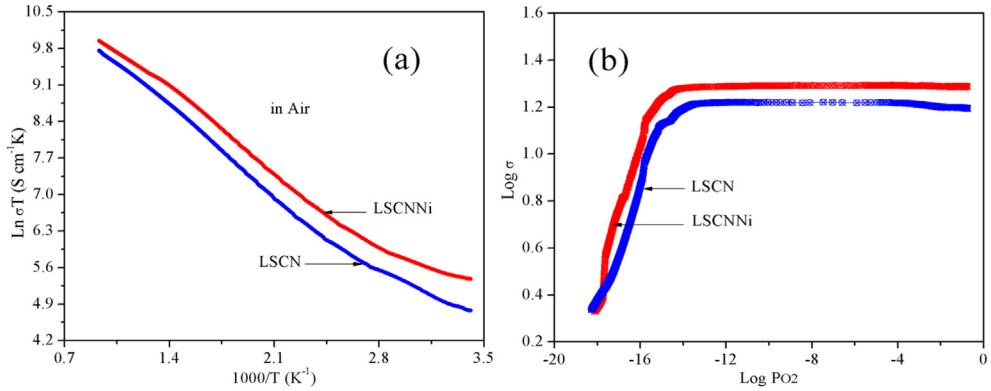

Fig. 5. The dependences of the conductivity of LSCN and LSCNNi on (a) the temperature in air from room temperature to 800 °C and in 5%H_2/Ar from 800 to 350 °C and (b) oxygen partial pressure ranging from 0.2 to 10^{-19} atm at 800 °C.

on the ceramic substrate. To validate the chemical change of reduced samples, TGA tests of the oxidized and reduced samples are performed in air from room temperature to 800 °C. Fig. 4(a) illustrates that the oxidized LSCN experiences a slight weight gain (approximately 0.1 wt%) below 200 °C and a slight weight loss at higher temperatures. For the reduced LSCN, a weight loss of 1.3 wt% is observed below 200 °C, owing to the loss of adsorbed water on the reduced LSCN sample. Above 200 °C, it experiences a weight gain of up to 0.8 wt% at 800 °C, which is probably due to the re-oxidation of the reduced sample. As shown in Fig. 4(b), a weight loss of 0.15 wt% occurred for the oxidized LSCNNi, which may be attributed to the loss of oxygen at higher temperatures. However, a dramatic weight gain of 1.75 wt% occurred up to 800 °C for the reduced LSCNNi. This is 0.95 wt% higher than the weight gain of 0.8 wt% for the reduced LSCN sample. The re-oxidation of the reduced LSCNNi sample, practically the oxidation of Ni to Ni^{2+}, contributes significantly to the 0.95 wt%weight gain, which is consistent with weight change of the reversible chemical reaction: $(La_{0.75}Sr_{0.25})_{0.95}(Cr_{0.8}Ni_{0.2})_{0.95}Ni_{0.05}O_{3-\delta} \leftrightarrow 0.05Ni + (La_{0.75}Sr_{0.25})(Cr_{0.8}Ni_{0.2})O_{3-\delta}$.

The dependence of the conductivity on temperature and oxygen partial pressure indicates that LSCN and LSCNNi are p-type electronic conductors. The temperature dependence of conductivity shows a typical semiconducting behavior having a positive coefficient with temperatures up to 800 °C in air as shown in Fig. 5(a).

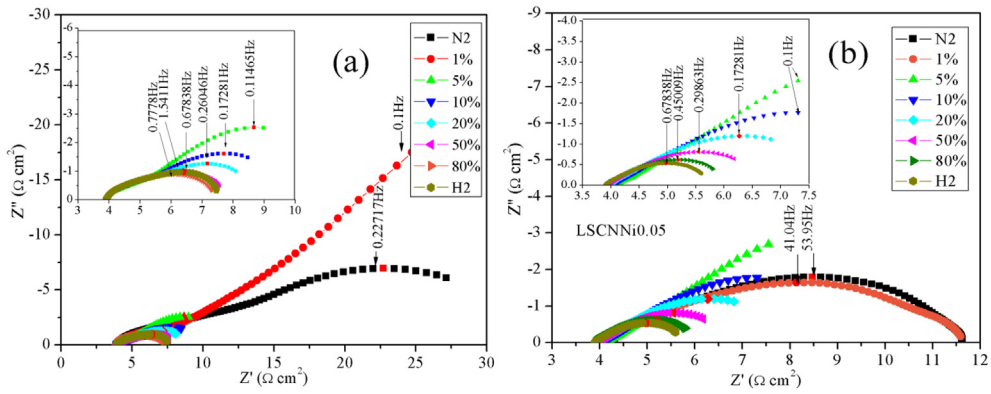

Fig. 6. AC impedances of the LSCN-SDC/YSZ/LSCN-SDC and LSCNNi-SDC/YSZ/LSCNNi-SDC symmetric cells tested at 800 °C at different hydrogen concentrations.

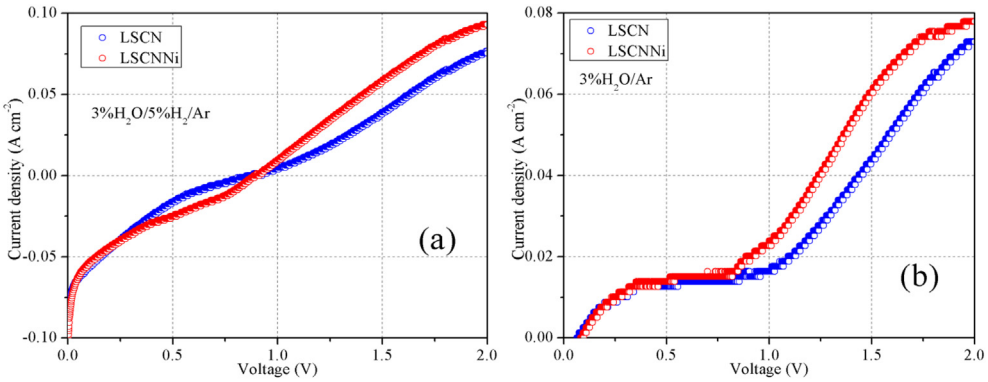

Fig. 7. Current–voltage (*I–V*) curves of the LSCN-SDC/YSZ/LSM-SDC and LSCNNi-SDC/YSZ/LSM-SDC electrolyzers at 800 °C with 3%H_2O/5%H_2/Ar and 3%H_2O/Ar supplying to the fuel electrode and the oxygen electrode exposing to air.

The conductivity of the LSCN reaches approximately 13 S cm^{-1} at 800 °C. The p-type conducting properties, displayed in Fig. 5(b), reveals that the conductivity of the LSCN sample is independent of the oxygen partial pressure when the log PO_2 is above 10^{-14} atm at 800 °C. However, the conductivity significantly decreases with the log PO_2 below 10^{-14} atm and finally reaches 2 S cm^{-1} at 10^{-18} atm. This is probably due to the decrease in the concentration of the charge carrier in reducing atmospheres. The oxygen partial pressure under strong reducing atmospheres greatly influences the conductivity of LSCN ceramic. This might be demonstrated in form of change of electrode polarizations in the process of steam electrolysis. In contrast, the perovskite LSCNNi with A-site deficiency and B-site excess demonstrates higher conductivity in air than LSCN ceramic. The conductivity of the LSCNNi reaches approximately 19 S cm^{-1} at 800 °C in air. The higher conductivity for LSCNNi in high oxygen partial pressure region is probably ascribed to enhanced p-type conduction, which is because the Ni-based solid oxide electrode materials normally demonstrate higher electronic conductivity than that of Cr-based materials at intermediate temperatures. A similar behavior of the dependence of conductivity on the oxygen partial pressure is observed. The conductivity of LSCNNi exhibits better property than LSCN. The anchored Ni nanoparticles in LSCNNi enhanced performance and thus improve the mixed conductivity in reducing atmospheres.

Fig. 6 presents the AC impedance spectra of the symmetric cells of LSCN/YSZ-YSZ-/LSCN/YSZ and LSCNNi/YSZ-YSZ-LSCNNi/YSZ tested at 800 °C at different hydrogen concentrations (0, 1, 5, 10, 20, 50, 80 and 100% H_2 in N_2). The intercept of the impedance spectra with the real axis at high frequency corresponded to the Ohmic resistance (Rs) of the cell, which mainly resulted from the

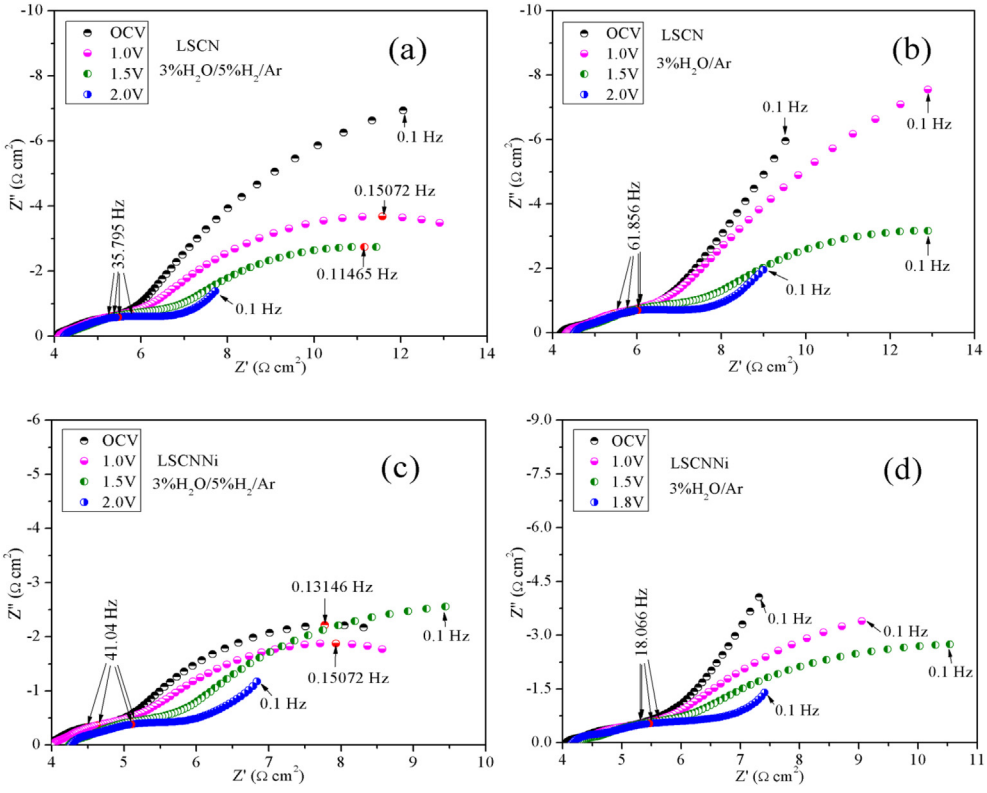

Fig. 8. AC impedances of the LSCN/YSZ-YSZ-LSM/YSZ and LSCNNi/YSZ-YSZ-LSCM/YSZ electrolyzers at different voltages in 3%H_2O/5%H_2/Ar at 800 °C.

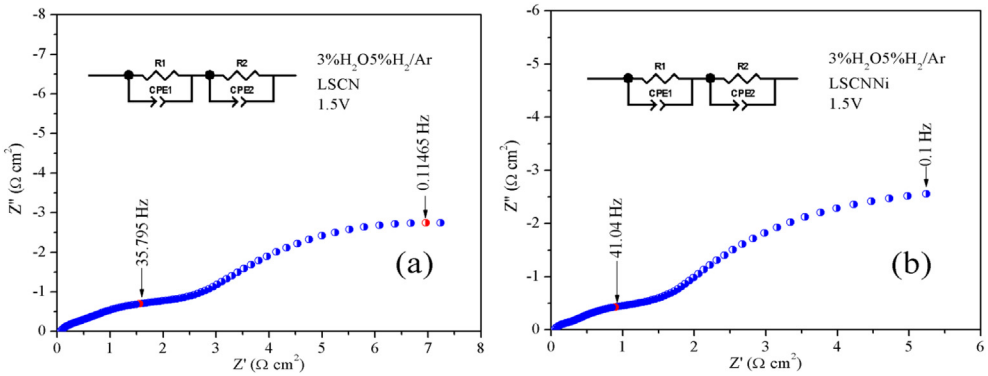

Fig. 9. Models of the in situ AC impedance of the solid oxide electrolyzer for steam electrolysis at 1.5 V in 3%H_2O5%H_2/Ar with (a) LSCN/YSZ and (b) LSCNNi/YSZ fuel electrodes at 800 °C.

ionic resistance of the YSZ electrolyte [29]. The intercept with the real axis at low frequency represents the total polarization resistance while the electrode polarization resistance (Rp) is the difference between two intercepts. The value of Rs is about 4 Ω cm^2 for both the LSCN/YSZ and LSCNNi/YSZ symmetric cells. However, the Rp significantly decreased with increasing hydrogen concentration, which is probably due to the enhanced electro-catalytic activity under strong reducing atmosphere. As shown in Fig. 6(a), the Rp of the symmetric cells based on LSCN/YSZ composite electrode is above 15 Ω cm^2 in pure N_2 and 1.8 Ω cm^2 in pure H_2. The symmetric cells based on LSCNNi/YSZ composite electrode exhibits similar phenomenon. The improved Rp under strong reducing atmosphere may be related to the high electro-catalytic activity of the composite fuel electrodes. However, it should be noted that LSCNNi/YSZ composite electrode shows better performance as it gives an improved Rp of only 0.9 Ω cm^2 in pure H_2 (Fig. 6(b)). It is probably due to the enhanced electro-catalytic activity of composite electrode by exsolving catalytic-active metallic Ni nano-particles.

The steam electrolysis is investigated on two solid oxide electrolyzers: (cathode) LSCN/YSZ-YSZ-LSM/YSZ (anode) and LSCNNi/YSZ-YSZ-LSM/YSZ at 800 °C with 3%H_2O/5%H_2/Ar and 3%H_2O/Ar supplied to the cathodes, respectively. Fig. 7(a) and (b) shows the typical curves of the voltage versus current density (I–V curves) of the electrolyzers. The open-circuit voltages (OCVs) of the electrolyzers are approximately 0.95 V and 0.13 V in 3%H_2O/5%H_2/Ar and 3%H_2O/Ar, respectively, which are consistent with H_2/O_2 fuel cell and the O_2/H_2O concentration cells, respectively [30]. The change in the slope of the I–V curves indicates that there exist two different cell processes in the two voltage regions: (a) the electrochemical reduction of the cathodes and oxidation of the anodes at low voltages; (b) the steam electrolysis at high voltages. As shown in Fig. 7(a), the current density reaches 0.093 A cm^{-2} at 2 V for the LSCNNi/YSZ cathode in 3%H_2O/5%H_2/Ar, while it is only 0.082 A cm^{-2} for the LSCN/YSZ cathode. This result is consistent with the above discussion about symmetrical cell performance, where the exsolution of Ni nano-particles under reducing atmosphere effectively improves the electro-catalytic performance. Similarly, as shown in Fig. 7(b), the current density reaches 0.078 A cm^{-2} at 2 V in 3%H_2O/Ar with the LSCNNi/YSZ cathode. However, a low current density of 0.070 A cm^{-2} is achieved for the cell with the LSCN/YSZ cathode. It is observed that a better electrode performance is obtained without a flow of reducing gas over the cathode, which can be explained as follows: the hydrogen generated in the cathode protects the catalytic-active Ni metal from oxidation while the catalyst simultaneously enhances the electrode performance. Nonetheless, it should be noted that the current densities in 3%H_2O/5%H_2/Ar are higher than that in 3%H_2O/Ar, which might be related to the better electro-catalytic performances of the cathode under stronger reducing atmospheres.

Fig. 8 shows the in situ AC impedance of the SOEs under a series of external voltages at 800 °C. The electrode polarization resistance, Rp, is considerably large at the low voltages. However, the increased voltages significantly activate the electrodes and decrease the Rp remarkably. To understand the electrode process, the AC impedance data at 1.5 V in 3%H_2O5%H_2/Ar with the LSCN and LSCNNi electrodes are modeled using an equivalent circuit. As shown in Fig. 9(a), the electrode process is assumed to be two arcs with the equivalent circuits (inserted). The value of R_1 is 3.00 Ω cm^2

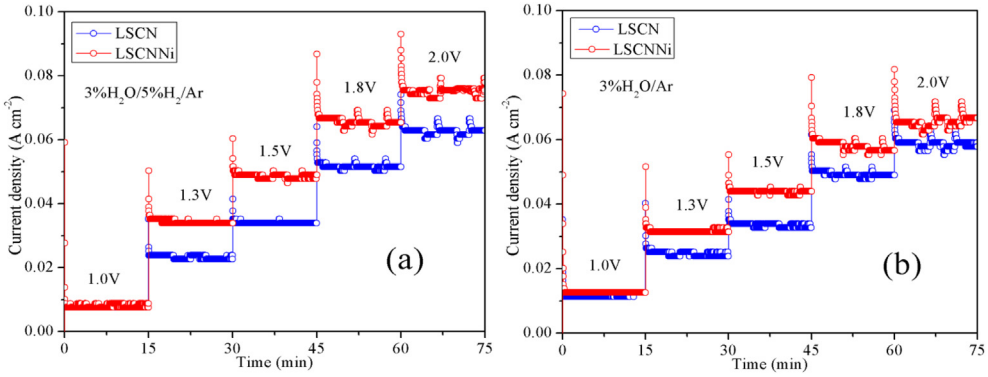

Fig. 10. Performance of the LSCN/YSZ-YSZ-LSM/YSZ and LSCNi/YSZ-YSZ-LSM/YSZ electrolyzers for steam electrolysis under different applied voltages in 3%H_2O/5%H_2/Ar and 3%H_2O/Ar at 800 °C.

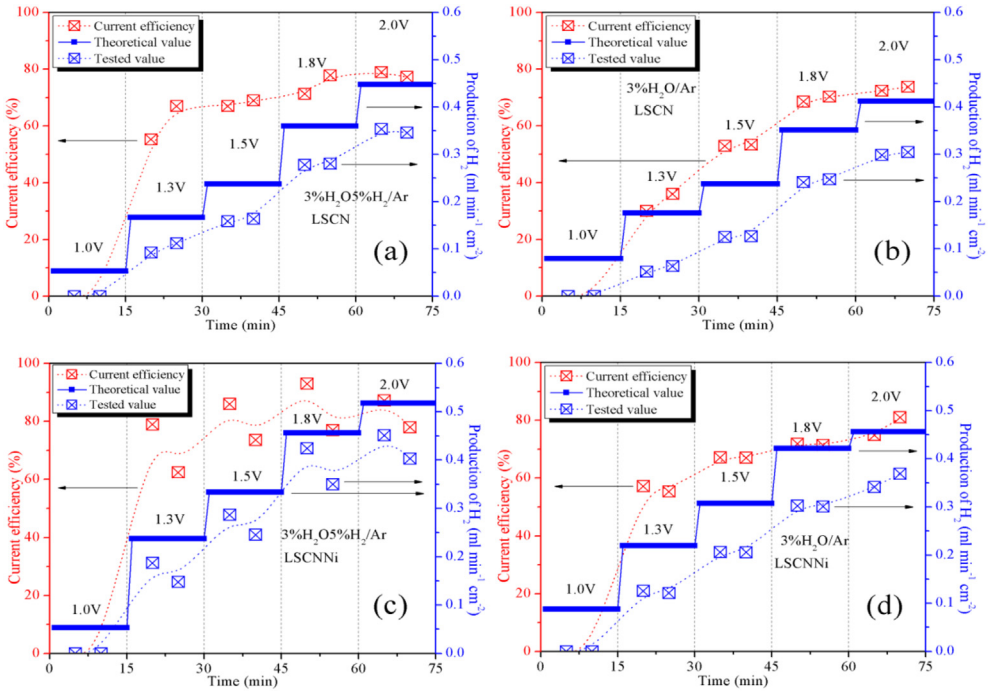

Fig. 11. H_2 production of and the current efficiency of the LSCN/YSZ-YSZ-LSM/YSZ and LSCNNi/YSZ-YSZ-LSM/YSZ electrolyzers for steam electrolysis under different applied voltages in 3%H_2O/5%H_2/Ar and 3%H_2O/Ar at 800 °C.

for the LSCN electrode, which implies a high frequency process and reflects the charge transfer between LSCN electrode and YSZ electrolyte. The R_2 reaches 8.57 Ω cm^2, which implies a low frequency process and includes the dissociative adsorption, the transfer of species at TPB and the surface diffusion [31,32]. In contrast, the R_1 reaches 2.01 Ω cm^2 for the LSCNNi electrode and the R_2 decreases to 6.64 Ω cm^2 as detailed in Fig. 9(b). This indicates that the exsolution of nickel metal improves the mixed conductivity (indicated by the high-frequency process), the dissociative adsorption, the transfer of species at TPB and surface diffusion (indicated by the low-frequency process). Two primary electrochemical processes appear in the range from OCV to 2 V during the steam electrolysis process: cathode reduction and steam electrolysis. The cathode reduction is the main process below 1.0 V while the steam electrolysis dominates the electrolysis process at high voltages.

In order to further understand the performance of the steam electrolysis process, the current densities are recorded against time at the applied voltages of 1.0, 1.3, 1.5, 1.8 and 2.0 V. The short-term performance of the SOEs in steam electrolysis at 800 °C under 3% H_2O/5%H_2/Ar and 3%H_2O/Ar atmosphere is as detailed in Fig. 10(a) and (b) respectively. Fig. 10(a) shows the current density versus the applied voltages for the SOE based on LSCN/YSZ or LSCNNi/YSZ electrodes with the flow of reducing gas over the cathode. The current density reaches approximately 0.62 A cm^{-2} at 2.0 V for the LSCN electrode. However, current density increases to 0.77 A cm^{-2} for the LSCNNi electrode. It is easy to find that the current density for the LSCNNi electrode is higher than that for the LSCN electrode at each applied voltage; Fig. 10(b) shows a similar pattern. The current density reaches approximately 0.58 A cm^{-2} at 2.0 V with the LSCN electrode, which is slightly lower than 0.67 A cm^{-2} for the LSCNNi electrode without reducing atmosphere. The better electrode performance in the process of direct steam electrolysis is attributed to the synergetic effect of the Ni catalyst and the ceramic LSCN electrode, which further confirms the results discussed above.

Fig. 11 shows H_2 production and the Faraday efficiency of the electrolyzers for steam electrolysis at the different applied voltages under the atmospheres of 3%H_2O/5%H_2/Ar and 3%H_2O/Ar at 800 °C, respectively. There is no H_2 production at 1.0 V because the

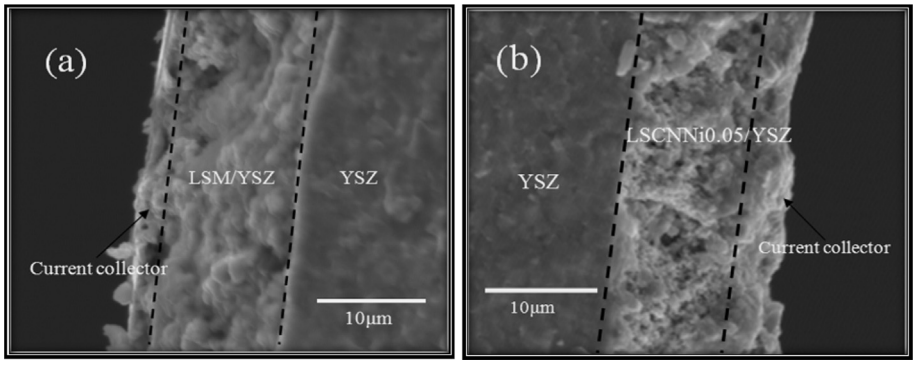

Fig. 12. SEM images of the tested solid oxide electrolyzers with the (a) LSM/YSZ composite electrode and (b) LSCNNi/YSZ composite electrode.

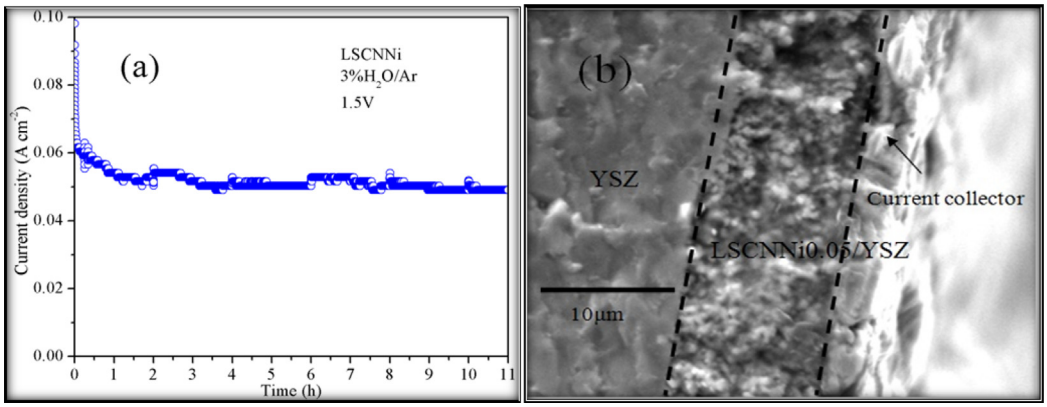

Fig. 13. (a) Performance of the SOE with LSCNNi/YSZ composite cathode for steam electrolysis at 800 °C for 11 h; (b) SEM image of the SOE after test.

electrolysis of H_2O does not start until 1.3 V. The maximum H_2 productions for the cell with LSCN/YSZ electrode as shown in Fig. 11(a) are 0.1117, 0.1634, 0.2801 and 0.3537 ml min^{-1} cm^{-2} at 1.3, 1.5, 1.8, and 2.0 V respectively, corresponding to the current efficiencies 67%, 69%, 77.9%, and 79%, respectively. For the LSCNNi/YSZ electrolyzer shown in Fig. 11(c), the maximum H_2 productions are 0.1871, 0.2866, 0.4242 and 0.4513 ml min^{-1} cm^{-2} at 1.3, 1.5, 1.8 and 2.0 V respectively, which are corresponding to the Faraday efficiencies 79%, 86%, 93%, and 87.2%, respectively. It can be seen that the Faraday efficiencies are enhanced by approximately 10% for the cell based on LSCNNi compared to the cell based on LSCN with reducing gas flowing over the cathodes. Fig. 11(b) and (d) shows that, without the reducing gas flowing over the cathodes, there is observable decrease in Faraday efficiencies at low voltages of the electrolyzer based on LSCN and LSCNNi. However, the applied potentials gradually enhance the cell performances as well as the Faraday efficiencies. The corresponding Faraday efficiencies reach 74% and 81% under the potential of 2.0 V for LSCN and LSCNNi cathodes respectively. Under ideal conditions, on the cathode side, H_2O molecule is reduced into H_2 with the electrons provided by the external circuit. The O^{2-} is completely transported through the oxygen-ion conducting electrolyte to the anode compartment, where O_2 gas is formed and released. However, the O^{2-} is not completely transported from the cathode side to the anode side under testing conditions because of the presence of tiny amount of hole conduction in electrolyte. On the hand, the small amount of gas leakage in cathode would consume part of the hydrogen, which is also expected to decrease the current efficiency.

The SEM image reveals the microstructure of the SOE with LSCNNi/YSZ cathode after steam electrolysis test. As shown in Fig. 12(a) and (b), a single SOE is constructed on YSZ electrolyte support with two porous composite electrodes. Both LSM/YSZ and LSCNNi/YSZ composite electrodes appear to have porous structures and adhere to the dense YSZ electrolyte notably well. The porous silver current collector layer is around 2 μm in thickness. To validate the stability of the LSCNNi/YSZ composite cathode, direct steam electrolysis is performed at a fixed voltage of 1.5 V and a temperature of 800 °C for 11 h without a flow of reducing gas on the cathode side. Fig. 13(a) reveals only a slight decrease in the current density (5–10%), within the first few hours. This is probably because the gas concentration is not at a proper equilibrium state during the change of atmosphere from 3%H_2O/5%H_2/Ar to 3%H_2O/Ar in the steam electrolysis process. On a general note, the current density is stable (approximately 0.05 A cm^{-2}). This indicates the stability of the LSCNNi/YSZ composite cathode in the H_2 generation from steam electrolysis. The synergetic effect of metallic catalyst and ceramic electrode leads to good stability as well as better performances of the composite cathodes without a flow of reducing gas. SEM image in Fig. 13(b) also provides the microstructure of the LSCNNi/YSZ cathode. There is no observable destructive phenomenon, and the porous composite cathode adheres well to the dense electrolyte, which further confirms the good stability of the LSCNNi/YSZ cathode for steam electrolysis.

4. Conclusion

The composite cathodes of LSCN/YSZ and LSCNNi/YSZ are methodically studied for steam electrolysis in oxygen-ion conducting solid oxide electrolyzers. The nickel exsolved from the A-site deficient and B-site excess LSCNNi, considerably improves the activity of the composite cathode. The exsolution of nano-metallic catalyst is reversible in redox cycles and the AC impedance test of the symmetric cells exhibits promising polarization resistance for the LSCNNi/YSZ cathode. The SOE with LSCNNi/YSZ cathode also exhibits good performances in either 3%H_2O/5%H_2/Ar or 3%H_2O/Ar at 800 °C. The cathode surface modification with an electrochemical catalytic nickel nano-particle leads to an enhanced current efficiency of about 10%. The collective effect of metallic catalyst and ceramic cathode produces good stability as well as better performances in the steam electrolysis. The present results provide remarkable evidence that, the LSCNNi would be good potential fuel electrode for direct steam electrolysis in an oxygen-ion conducting solid oxide electrolyzer.

Appendix A. Supplementary data

Supplementary data related to this article can be found at http://dx.doi.org/10.1016/j.jpowsour.2013.07.082.

References

[1] M.I. Hoffert, K. Caldeira, G. Benford, D.R. Criswell, C. Green, H. Herzog, A.K. Jain, H.S. Kheshgi, K.S. Lackner, J.S. Lewis, H.D. Lightfoot, W. Manheimer, J.C. Mankins, M.E. Mauel, L.J. Perkins, M.E. Schlesinger, T. Volk, T.M.L. Wigley, Science 295 (2002) 981–987.
[2] K. Xie, Y.Q. Zhang, G.Y. Meng, J.T.S. Irvine, Energy Environ. Sci. 4 (2011) 2218.
[3] K. Xie, N. Umezawa, N. Zhang, P. Reunchan, Y.J. Zhang, J.H. Ye, Energy Environ. Sci. 4 (2011) 4211.
[4] J.S. Herring, J.E. O'Brien, C.M. Stoots, G.L. Hawkes, J.J. Hartvigsen, M. Shahnam, Int. J. Hydrogen Energy 32 (2007) 440.
[5] X.D. Yang, J.T.S. Irvine, J. Mater. Chem. 18 (2008) 2349.
[6] R.M. Xing, Y.R. Wang, S.H. Liu, C. Jin, J. Power Sources 208 (2012) 276.
[7] K. Xie, Y.Q. Zhang, G.Y. Meng, J.T.S. Irvine, J. Mater. Chem. 21 (2011) 195.
[8] G. Tsekouras, J.T.S. Irvine, J. Mater. Chem. 21 (2011) 9367.
[9] S.S. Li, Y.X. Li, Y. Gan, K. Xie, G.Y. Meng, J. Power Sources 218 (2012) 244.
[10] S.S. Xu, S.G. Chen, M. Li, K. Xie, Y. Wang, Y.C. Wu, J. Power Sources 239 (2013) 332–340.
[11] T. Ishihara, N. Jirathiwathanakul, H. Zhong, Energy Environ. Sci. 3 (2010) 665.

[12] F. Bidrawn, G. Kim, G. Corre, J.T.S. Irvine, J.M. Vohs, R.J. Gorte, Electrochem. Solid-State Lett. 11 (2008) B167.
[13] B. Yu, W.Q. Zhang, J. Chen, J.M. Xu, S.R. Wang, Sci. China Ser. B Chem. 51 (2008) 289–304.
[14] K.F. Chen, N. Ai, S.P. Jiang, Int. J. Hydrogen Energy 37 (2012) 10517.
[15] S.S. Li, Q.Q. Qin, K. Xie, Y. Wang, Y.C. Wu, J. Mater. Chem. A, http://dx.doi.org/10.1039/C3TA10404D.
[16] S.D. Ebbesen, R. Knibbe, M. Mogensen, J. Electrochem. Soc. 159 (2012) F482.
[17] S.D. Ebbesen, M. Mogensen, J. Power Sources 193 (2009) 349.
[18] Z.W. Wang, M. Mori, T. Itoh, J. Fuel Cell Sci. Technol. 9 (2012) 021004, 1.
[19] J.H. Kim, D. Miller, H. Schlegl, D. McGrouther, J.T.S. Irvine, Chem. Mater. 23 (2011) 3841.
[20] E.S. Raj, J.A. Kilner, J.T.S. Irvine, Solid State Ionics 177 (2006) 1747.
[21] S.M. Plint, P.A. Connor, S.W. Tao, J.T.S. Irvine, Solid State Ionics 177 (2006) 2005–2008.
[22] S.S. Xu, S.S. Li, W.T. Yao, D.H. Dong, K. Xie, J. Power Sources 230 (2013) 115–121.
[23] S.W. Tao, J.T.S. Irvine, Nat. Mater. 2 (2003) 320.
[24] J. Sfeir, P.A. Buffat, P. MÖckli, N. Xanthopoulos, R. Vasquez, H.J. Mathieu, J.V. Herle, K.R. Thampi, J. Catal. 202 (2001) 229–244.
[25] S.W. Tao, J.T.S. Irvine, Chem. Mater. 16 (2004) 4116–4121.
[26] S. Lee, G. Kim, J.M. Vohs, R.J. Gortea, J. Electrochem. Soc. 155 (2008) B1179–B1183.
[27] A.L. Sauvet, J.T.S. Irvine, Solid State Ionics 167 (2004) 1–8.
[28] V.B. Vert, F.V. Melo, L. Navarrete, J.M. Serra, Appl. Catal. B Environ. 115–116 (2012) 346–356.
[29] C. Jin, C.H. Yang, F. Zhao, D. Cui, F.L. Chen, Int. J. Hydrogen Energy 36 (2011) 3340.
[30] C. Wagner, Z. Phys. Chem. 42 (1933) B41.
[31] Y. Gan, J. Zhang, Y.X. Li, S.S. Li, K. Xie, J.T.S. Irvine, J. Electrochem. Soc. 159 (2012) F763–F767.
[32] M.J. Jorgensen, M. Mogensen, J. Electrochem. Soc. 148 (2001) A433.